Transient Cooling Model for Rapid Chilled-Water Generation in a Single-tank Chiller–Heat Exchanger System

Nopparat Katkhaw, Wichaphon Fakkeaw, Sutham Arun, and Rachaneewan Aungkurabrut *

School of Engineering, University of Phayao, Phayao, Thailand
Email: nopparat.ka@up.ac.th (N.K.); wichaphon.fa@up.ac.th (W.F.); sutham.ar@up.ac.th (S.A.); rachaneewan.ch@up.ac.th (R.A.)
*Corresponding author

Abstract*—This paper addresses the industrial challenge of sizing chiller capacity in rapid chilled-water generation systems under limited cooling time windows. The core heat transfer challenge lies in the transient nature of single-tank configurations; under low Richardson number (Ri) conditions, mixing-dominated behavior occurs, to eliminate the steady temperature differences assumed in conventional sizing methods. To address this, this study develops an explicit analytical model based on a quasi-steady-state heat transfer assumption, which is physically justified by the large mismatch in thermal time constants between the water tank and the heat exchanger. The model was validated experimentally using a 3-kW mini-chiller, a 60-L tank, and a plate heat exchanger across four flow-rate conditions. The experimental results support the use of the quasi-steady-state heat transfer assumption within the system. Furthermore, while the heat exchanger effectiveness varies continuously over time due to changes in operating conditions, it can be represented by a time-averaged value because the narrow operating temperature range produces limited variations in the thermophysical properties of water. Finally, the empirical data indicate mixing-dominated conditions at low Ri values, under which the proposed transient cooling model reasonably predicts the bulk temperature decline, with R^2 values ranging from 0.8738 to 0.9978 across the tested conditions. The resulting non-dimensional NTU–effectiveness design equation provides a practical basis for first-pass chiller and heat exchanger sizing in rapid chilled-water generation systems operating under similar mixed-tank conditions.

***Keywords*—chiller sizing, tank-based cooling system, rapid cooling, thermal mixing**

I. Introduction

Chilled water plays a vital role in various industrial processes, including air-conditioning systems, cooling of metal workpieces in high-temperature casting or rolling operations, waterjet cutting machines, low-heat concrete production, and cold-water aquaculture systems, among others [1]. In conventional chilled water systems, the chiller reduces the water temperature and delivers it directly to the process. In systems that utilize a cold water storage tank, the chiller cools the water by continuously circulating it from the tank through the chiller and back until the desired temperature is achieved.

Additionally, most chilled water systems require the addition of chemical agents to maintain water quality—including pH control, scale prevention in pipelines and heat exchangers, and microbial growth inhibition—rendering the chilled water unsuitable for direct contact with the end product in certain applications. In cold-water aquaculture, chilled water must be prepared in advance for water replacement, while in low-heat concrete production, chilled water is mixed directly with cement at a target temperature of approximately 10–15 °C [2, 3]. According to operator reports, chilled water must typically be produced within approximately 30 minutes to meet process requirements. To address these constraints, the chilled water system must be segregated into two loops as a primary loop and a secondary loop with heat exchanged between them through a heat exchanger, as illustrated in Fig. 1.

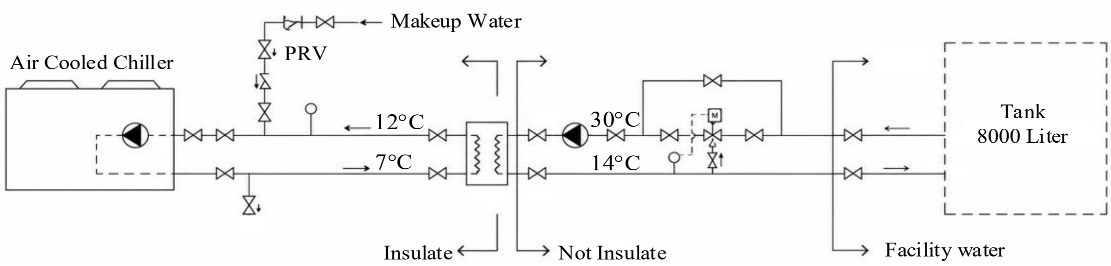

Fig. 1. A sample of a chilled water generation system.

Manuscript received February 25, 2026; revised April 23, 2026; accepted June 29, 2026; published September 8, 2026.

Although optimal cooling performance is achieved with the separation of the warm water tank and the chilled water storage tank, installing two large tanks independently leads to significantly higher costs and increased space requirements. Therefore, producing chilled water within a single tank presents a feasible and space-saving alternative. In the design of chilled water systems for tank-based cooling, determining the required size of the chiller or heat exchanger is relatively straightforward when the system utilizes separate tanks or when clear thermal stratification occurs within the tank. In such cases, engineers often rely on basic engineering principles, such as the heat transfer equation $Q = \dot{m}C_p\Delta T$ [4, 5]. However, in single-tank systems that require rapid cooling, complete thermal mixing occurs between the warm and chilled water, which eliminates the steady temperature difference normally assumed in conventional sizing methods. As a result, both the cooling capacity of the chiller and the effectiveness of the heat exchanger vary continuously with the declining tank temperature—an inherently transient behavior that increases the complexity of chiller and heat exchanger sizing. Consequently, applying simplified steady-state equations without proper consideration of this transient nature leads to inaccurate chiller sizing, which can adversely affect the efficiency and continuity of industrial processes.

Research on chilled-water storage has largely centered on air-conditioning applications, especially in the area of stratified thermal energy storage. Earlier work examined how tank shape, diffuser configuration [6–8], and internal flow management [9–13] influence the formation and stability of the thermocline. Several studies have also described how the inlet velocity and temperature difference interact to suppress or promote mixing once a thermocline is established [14]. Additional modeling efforts investigated how charging flow rate and tank geometry alter the stratification curve [15], while others highlighted the importance of the Richardson number (Ri) for characterizing thermocline quality and its sensitivity to discharge or charging flow conditions [16–18].

Even though Ri has been validated as a useful indicator of stratification quality, most of the existing work focuses on situations in which Ri remains high, and the thermal layers are allowed to form and persist for extended durations. These conditions are remarkably different from rapid chilled-water generation, where mixing is intentional, the Richardson number is low, and the cooling window is short. While the stratification literature provides strong insight into layered storage behavior, it offers limited guidance for tanks that can be modeled as fully mixed volumes. More importantly, it does not describe how the declining temperature difference inside the tank or the time-dependent effectiveness of a heat exchanger should be represented when predicting cooling performance. As a result, steady-state heat-transfer equations—commonly used in practice—do not adequately reflect the transient nature of rapid cooling and can lead to underestimated chiller capacity.

Beyond stratified storage, studies on more complex energy systems have used transient simulation tools to evaluate multi-loop configurations. Renewable-driven polygeneration systems have been analyzed through dynamic modeling and optimization to coordinate electricity, heating, cooling, and hydrogen production [19]. Similar approaches have been applied to solar-assisted, grid-tied systems designed for transportation and energy storage applications, where thermal storage interacts with several subsystems under varying operating conditions [20]. In addition, solar-assisted absorption cooling systems have been examined to understand temperature evolution across multiple loops that include collectors, thermal storage, chillers, and building loads [21]. These studies provide a system-level understanding of performance but do not yield analytical expressions for sizing a chiller or heat exchanger in a single-tank, mixing chilled-water system where the effectiveness varies as the water temperature decreases.

From the currently reviewed literature, no analytical sizing methodology explicitly addresses single-tank, two-loop chilled water systems operating under mixing and transient conditions. Existing steady-state methods may underestimate the required chiller capacity as they tend to assume constant temperature differences, while available transient models either require numerical solution or do not account for the continuous variation in heat exchanger effectiveness as the tank cools. This gap is particularly problematic for rapid cooling applications with limited duration for the cooling process, and where accurate first-pass sizing is essential to avoid costly oversizing or process delays due to undersizing.

To bridge the gap between idealized steady-state calculations and real transient behavior, the present work develops a mathematical modeling framework for a two-loop rapid chilled-water system. The core theoretical challenge involves coupling the transient bulk-temperature decline of the water tank with the heat exchanger equations, which are commonly applied under steady-state conditions. This challenge is addressed by adopting a quasi-steady-state heat transfer assumption. The assumption is physically supported by the large mismatch in thermal time constants between the system components. While the water tank has a substantial thermal mass that cools gradually over the designated cooling window, the heat exchanger contains a relatively small fluid inventory that responds over a much shorter time scale. The resulting framework represents the transient system dynamics through this quasi-steady behavior and provides an explicit analytical basis for first-pass chiller and heat exchanger sizing in rapid chilled-water generation systems. The remainder of this paper is organized as follows: Section II presents the system analysis, the mathematical formulation of the transient temperature model, the experimental configuration, and the uncertainty analysis. Section III presents the experimental results and validation. Section IV discusses the model's applicability and engineering implications, and Section V summarizes the concluding remarks.

II. Analysis

A. System Analysis

This section presents a dynamic thermal model for predicting the transient temperature of a mixing chilled-water tank by incorporating time-dependent heat exchanger effectiveness within the NTU–effectiveness framework. The present model incorporates a time-varying heat-exchanger effectiveness and links it with a transient energy balance of a mixed tank, allowing the cooling behavior to be predicted under realistic, non-steady operating conditions. The model is formulated to describe the cooling behavior of a single-tank, two-loop chilled-water generation system operating under mixing conditions.

Consider a chilled water generation system designed to rapidly cool the water stored in a tank. The system consists of two circulation loops—a primary loop linking the chiller to the heat exchanger and a secondary loop linking the tank to the heat exchanger. The water is cooled within the tank using a mini chiller through a heat exchanger. To achieve a high chilled-water charging rate, it is assumed that the temperature distribution within the tank is uniform without thermal stratification, as illustrated in Fig. 2.

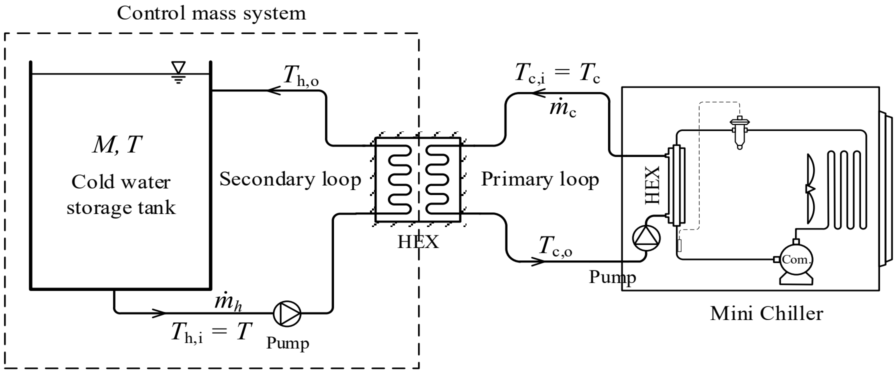

Fig. 2. Chilled water generation system.

The heat-transfer analysis of the system can be expressed as follows:

1) Energy exchange through the heat exchanger

To describe the heat transfer process, the mass of water in the tank is M with an initial temperature of T_0. Water from the tank is pumped into a heat exchanger at a mass flow rate $\dot{m}_h$. Since mixing is assumed to occur within the tank, the inlet temperature to the heat exchanger from the tank, $T_{h,i}$, is equal to the tank temperature T. Upon exiting the heat exchanger, the water temperature decreases to $T_{h,o}$.

At this point, the flow configuration of the system is separated into two circulation loops:

- the secondary loop, which circulates water between the tank and the heat exchanger at a flow rate of $\dot{m}_h$, and
- the primary loop, which circulates chilled water between the chiller and the heat exchanger at a flow rate of $\dot{m}_c$.

2) Assumption for the analytical model

To represent the tested operating conditions, several simplifying assumptions are adopted in the proposed model to maintain analytical tractability, and their implications are as follows:

- The chiller outlet temperature (T_c) remains constant throughout the cooling process.
- The model assumes that the tank is perfectly insulated and, therefore, heat gain from the surrounding environment is neglected.
- The thermal mass of the piping network connecting the tank, pump, and heat exchanger is not accounted for in the energy balance.
- The heat addition from the circulation pump is treated as negligible in the present formulation.

The water temperature exiting the mini chiller is assumed to remain constant at T_c. Therefore, the chilled water enters the heat exchanger at $T_{c,i} = T_c$ and exits at $T_{c,o}$.

Using these inlet and outlet conditions, the heat transfer rate across the heat exchanger can be evaluated from an energy balance:

$$Q = \dot{m}_h C_p (T - T_{h,o}) = \dot{m}_c C_p (T_{c,o} - T_c) \tag{1}$$

where C_p is the specific heat capacity of water. An alternative expression may be obtained by relating the total heat transfer rate to the Log Mean Temperature Difference (LMTD), denoted as ΔT_m :

$$Q = UA\,\Delta T_m \tag{2}$$

where U is the overall heat transfer coefficient, and A is the heat exchange area. The LMTD is defined as

$$\text{LMTD} = \Delta T_m = \frac{\left(T - T_{c,o}\right) - \left(T_{h,o} - T_c\right)}{\ln\left(\frac{T - T_{c,o}}{T_{h,o} - T_c}\right)} \tag{3}$$

Eqs. (1)–(3) may be applied to instantaneous heat transfer provided that the system operates in a quasi-steady state. This assumption is reasonable when the mass flow rates ($\dot{m}_h$ and $\dot{m}_c$) are sufficiently high, causing the thermal response time of the heat exchanger to become significantly shorter than the time scale of the transient fluctuations. Under these conditions, the convective heat transfer coefficients are high enough that the thermal inertia of the heat exchanger wall has a negligible effect on the overall transient response.

3) NTU–effectiveness relation and transient behavior

The steady-state heat exchanger effectiveness is traditionally defined as the ratio of the actual heat transfer rate to the maximum possible heat transfer rate. To account for transient thermal behavior, we define the instantaneous effectiveness, $\varepsilon(t)$, as:

$$\varepsilon(t) = Q(t)/Q_{max}(t) \tag{4}$$

where the maximum possible heat transfer rate, for heat exchange with the same fluid type in both loops, is given by

$$Q_{max}(t) = \dot{m}_{\min} C_p (T(t) - T_c) \tag{5}$$

Here, $\dot{m}_{\min} = \min(\dot{m}_h, \dot{m}_c)$ is the smaller of the two mass flow rates, and the temperature difference is taken between the hot and cold fluid inlets. From Eq. (1), it follows that

$$\varepsilon(t) = \frac{\dot{m}_h C_p \left(T(t) - T_{h,o}(t)\right)}{\dot{m}_{\min} C_p (T(t) - T_c)} \tag{6}$$

Consequently, the actual heat transfer rate can be determined from known input conditions as:

$$Q(t) = \varepsilon(t) \dot{m}_{\min} C_p (T(t) - T_c) \tag{7}$$

For a heat exchanger with the same fluid type in both loops, the effectiveness can alternatively be determined as a function of NTU and the heat capacity ratio C_r, as follows [22, 23]:

$$\varepsilon(t) = f(\mathrm{NTU}(t), Cr) \tag{8}$$

where

$$\mathrm{NTU}(t) = \frac{U(t)A}{\dot{m}_{\min} C_p} \tag{9}$$

$$C_r = \frac{\min(\dot{m}_h, \dot{m}_c)}{\max(\dot{m}_h, \dot{m}_c)} \tag{10}$$

In these expressions, U is the overall heat transfer coefficient, and A is the heat exchange area. Because $U(t)$ varies with the water temperature during cooling, the NTU also changes over time.

4) Transient temperature model of the mixing phenomena tank

For the analysis of the cooling behavior of the tank, the water and piping are treated as a control-mass system since no chilled water is withdrawn during the production phase. Under this assumption, the transient temperature of the tank is governed by an energy balance between the tank water and the heat exchanger. The rate of temperature change of the water in the tank is expressed as

$$M\frac{dT}{dt} = -\varepsilon(t)\dot{m}_{\min}(T(t) - T_c) \tag{11}$$

Eq. (11) represents the fundamental dynamic relation for the mixed tank when the temperature decreases proportionally to the temperature difference ($T(t) - T_c$), scaled by the time-varying effectiveness $\varepsilon(t)$.

Since T_c is assumed constant, the equation can be rearranged by separating variables:

$$-\frac{1}{T-T_c} d(T - T_c) = \frac{\dot{m}_{min}}{M} \varepsilon(t)dt \tag{12}$$

This separation isolates the temperature-dependent term on the left-hand side and the time-dependent effectiveness on the right-hand side, preparing the equation for integration.

Integrating both sides from $t = 0$ to t, with initial tank temperature T_0, yields:

$$\ln\left(\frac{T_0 - T_c}{T - T_c}\right) = \frac{\dot{m}_{min}}{M} \int_0^t \varepsilon(t)dt \tag{13}$$

Eq. (13) expresses the tank temperature implicitly as a function of the accumulated effectiveness over time. By defining the time-dependent accumulated effectiveness, $E(t)$, as:

$$E(t) = \int_0^t \varepsilon(t)dt, \quad \varepsilon(t) = \frac{dE(t)}{dt} \tag{14}$$

the explicit solution becomes:

$$T = T_c + (T_0 - T_c) \cdot \exp\left[-\frac{\dot{m}_{min}}{M}(E(t))\right] \tag{15}$$

This closed-form expression directly links the tank temperature to the time-dependent heat exchanger effectiveness, enabling the prediction of cooling dynamics for any prescribed $\varepsilon(t)$ variation. Furthermore, if the time-averaged effectiveness is defined as $\bar{\varepsilon} = \frac{1}{t_f}\int_0^{t_f} \varepsilon(t)dt$ the final temperature at time t_f is given by:

$$T_f = T_c + (T_0 - T_c) \cdot \exp\left[-\frac{\dot{m}_{min}}{M}\bar{\varepsilon} t_f\right] \tag{16}$$

5) Conditions for validity for a mixing tank assumption

In this study, we assume no thermal stratification within the tank. To ensure that this assumption is physically valid for the conditions under which Eq. (16) is applied, the Richardson number (Ri) is used as a criterion for assessing the degree of mixing inside the tank.

The Richardson number, defined as the ratio between buoyancy force and mixing force, indicates the tendency of thermal stratification in the chilled-water tank. A high Richardson number implies significant stratification potential, whereas a low Richardson number indicates thorough mixing and negligible stratification.

If chilled water flows into the tank through an inlet pipe at velocity u_{in}, and the tank itself has a height H, then the highest possible water temperature in the tank corresponds to the initial water temperature T_0, while the lowest possible temperature corresponds to the temperature of chilled water entering the heat exchanger, T_c. Thus, the Richardson number can be expressed as follows:

$$\mathrm{Ri} = \frac{g\beta H(T_0 - T_c)}{u_{in}^2} \tag{17}$$

where:
g = gravitational acceleration,
β = coefficient of thermal expansion,
H = tank height
T_0 = initial tank temperature
T_c = chilled water supply temperature from the chiller
u_{in} = inlet velocity

This criterion allows the applicability of the mixing assumption to be evaluated, ensuring that the transient temperature model remains valid only under conditions where mixing dominates over stratification.

B. Experimental Setup

An experimental setup was constructed as provided in Fig. 3. The system comprised a 3-kW mini chiller that employed a capillary tube to reduce refrigerant pressure. This configuration resulted in a gradual decrease in the chilled water outlet temperature rather than a stable supply temperature. To stabilize the temperature entering the heat exchanger, a chilled water storage tank was installed. This tank was used to approximate the nearly constant T_c condition assumed in the model. The heat exchanger was a plate-type SWEP model B5THx8/1P-SC-M. Water circulation through the heat exchanger was achieved using both primary and secondary pumps.

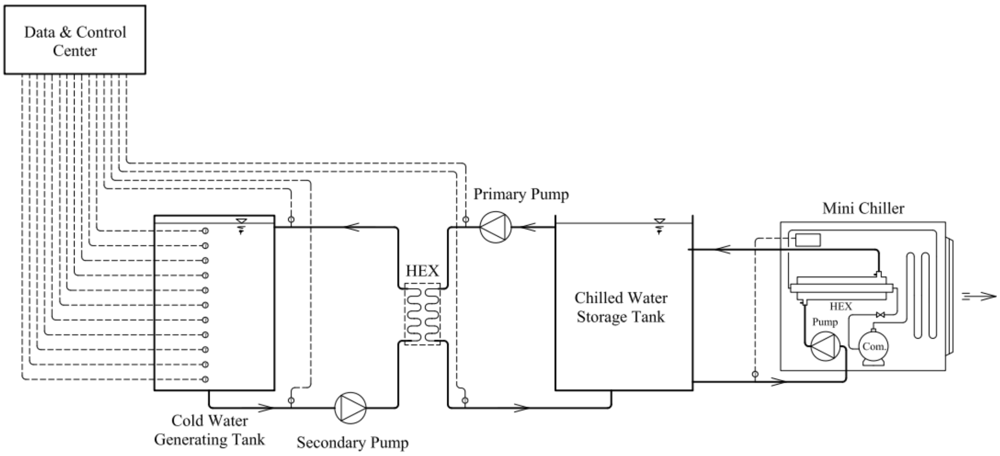

(a)

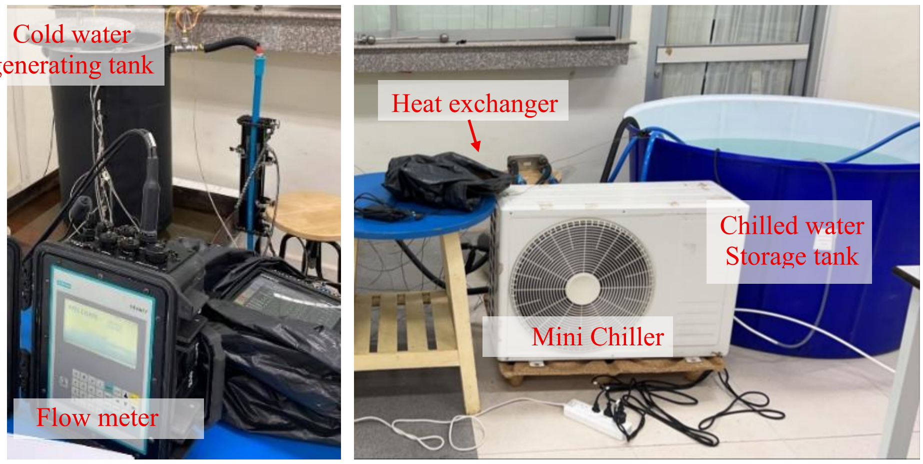

(b)

Fig. 3. The experimental setup: (a) schematic diagram of the cold-water generation system; (b) photographs of the experimental setup.

This experimental work aims to identify the heat exchanger's transient characteristics and to validate the transient temperature model of the mixing phenomena presented in Eq. (15). To achieve this, temperatures were measured at the inlet and outlet of the plate heat exchanger, and an ultrasonic flow meter was installed on the secondary loop to monitor the water flow rate. Additionally, ten thermocouples were distributed along the vertical axis of the tank to monitor the cooling behavior and thermal stratification. Temperature was measured using type-K thermocouples connected to a GRAPHTEC midi LOGGER GL840.

To minimize heat loss to the surroundings, the cold-water generating tank was fully insulated with a closed-cell elastomeric material, and all piping connections were wrapped with thermal insulation. Moreover, all experiments were conducted in an air-conditioned room maintained at 25 °C to ensure a stable ambient temperature throughout the test period.

In the experiment, the chilled water storage tank was first cooled to a temperature of approximately 7–9 °C and maintained at that level using the mini chiller. The water in the cold-water generating tank was then heated to a temperature range of 30–35 °C. The experiment commenced by activating both the primary and secondary pumps, with the flow rate through the secondary pump controlled to be lower than that of the primary pump ($\dot{m}_{\mathrm{min}} = \dot{m}_{\mathrm{h}}$). Water flow rates, inlet and outlet temperatures of the heat exchanger, as well as temperatures within the tank, were recorded at one-minute intervals. A total of four experimental runs were conducted, each with a different value of mass flow rate $\dot{m}_{\mathrm{h}}$.

C. Experimental Error Analysis

The error in experimental measurements is typically defined as the possible deviation between the measured and true values. According to Moffat [24], the overall uncertainty in a calculated result R, which is a function of multiple measured variables, can be expressed as:

$$R = R(X_1, X_2, X_3, ..., X_N) \tag{18}$$

where $X_1, X_2, ...$ are measured variables.

If uncertainty is associated with a single variable X_1, its contribution to the uncertainty in R is given by

$$\delta R_i = \frac{\partial R}{\partial X_i}\delta X_i \tag{19}$$

For multiple independent variables, the total uncertainty in R can be obtained using the root-sum-square (RSS) method:

$$\delta R = \left\{\sum_{i=1}^{N}\left(\frac{\partial R}{\partial X_i}\delta X_i\right)^2\right\}^{\frac{1}{2}} \tag{20}$$

The relative uncertainty is defined as

$$e = \frac{\delta R}{R} = \left\{\sum_{i=1}^{N}\left(\frac{1}{R}\frac{\partial R}{\partial X_i}\delta X_i\right)^2\right\}^{\frac{1}{2}} \tag{21}$$

The resulting uncertainty values were used to support the model-deviation analysis presented in Table I. The temperature uncertainty was taken as ±1% for the type-K thermocouple measurements, and the flow-rate uncertainty was taken as ±2% for the ultrasonic flow meter, based on the manufacturer's specifications. Because $\dot{m}_{\mathrm{min}} = \dot{m}_{\mathrm{h}}$, the measured secondary-loop flow rate was used in the uncertainty propagation. The equivalent thermal mass used in the transient temperature model was treated as constant because it was determined from fixed water and tank masses and fixed specific heat values.

TABLE I. UNCERTAINTY BUDGET FOR CALCULATED QUANTITIES

Calculated quantity	Variables included in propagation	Constants treated as fixed	Estimated uncertainty	Dominant contributor
Tank temperature prediction, T(t)	T_0, T_{c}, $\dot{m}_{\mathrm{h}}$, $\bar{\varepsilon}$	Equivalent thermal mass, C_p	2.8–5.5%	Temperature measurement and averaged effectiveness
Richardson number, Ri	T_0, T_{c}, $\dot{m}_{\mathrm{h}}$ through u_{in}	g, β, H, inlet diameter	4.5–5.0%	Inlet velocity from flow rate
Experimental effectiveness, ε	$T_{\mathrm{h,i}}$, $T_{\mathrm{h,o}}$, $T_{\mathrm{c,i}}$	$\dot{m}_{\mathrm{min}} = \dot{m}_{\mathrm{h}}$; flow-rate term cancels	2.6%	Temperature-difference measurement
NTU-based effectiveness	$T_{\mathrm{h,i}}$, $T_{\mathrm{h,o}}$, $T_{\mathrm{c,i}}$, $T_{\mathrm{c,o}}$, $\dot{m}_{\mathrm{h}}$ through Q, LMTD, UA, and NTU	C_p	5.3%	LMTD temperature differences

For the heat exchanger effectiveness calculated from Eq. (6), $\dot{m}_{\mathrm{min}} = \dot{m}_{\mathrm{h}}$; therefore, the flow-rate term cancels out. The propagated uncertainty was evaluated from $T_{\mathrm{h,i}}$, $T_{\mathrm{h,o}}$, and $T_{\mathrm{c,i}}$. For the NTU-based effectiveness, the uncertainty was propagated through the sequential calculations of Q, LMTD, UA, NTU, and ε. Because UA was calculated from Q/LMTD, its uncertainty was implicitly determined from the measured temperatures and secondary-loop flow rate. The uncertainty in the Richardson number was evaluated from T_0, T_{c}, and $\dot{m}_{\mathrm{h}}$ through the inlet velocity. For the transient tank-temperature prediction, the uncertainty propagation included T_0, T_{c}, $\dot{m}_{\mathrm{h}}$, and the time-averaged effectiveness used in Eq. (15), while the equivalent thermal mass and C_p were treated as constants.

Because each flow-rate condition was recorded as a single continuous transient time series, measurement consistency was assessed from the scatter of the measured effectiveness around the fitted $\varepsilon(t)$ curve and from the spatial consistency of thermocouples T2–T10 used to calculate the tank-averaged validation temperature. The resulting uncertainty values were used to support the model-deviation analysis presented in Table I.

Fig. 4 provides an overview of the complete methodology used in this study, summarizing the experimental procedures, data acquisition steps, and computational processes required for determining heat-exchanger effectiveness, evaluating mixing conditions, and validating the transient temperature model.

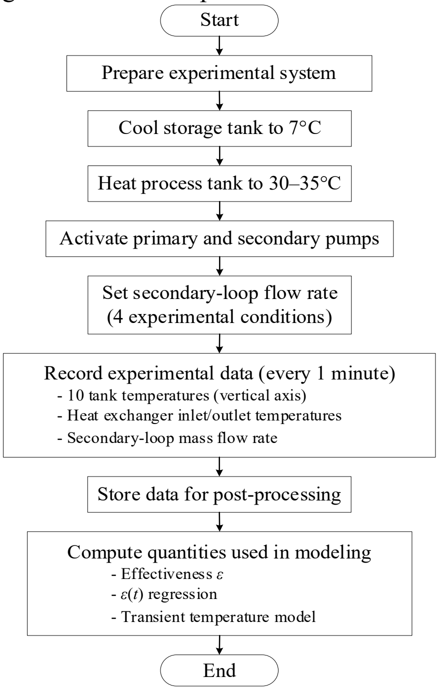

Fig. 4. Experimental procedure and data acquisition workflow for calculating effectiveness and validating the transient tank temperature model.

III. Experimental Result

A. Experimental Conditions and Objectives

The experimental program was structured around two primary objectives. First, a phenomenological study was conducted to verify the fundamental physical laws and assumptions of the model, such as the quasi-steady-state behavior and the threshold of thermal stratification relative to the Richardson number (Ri). For this purpose, data from all four experiments (Table II) were utilized to ensure consistent verification across a broad operating range. Second, a predictive mathematical model was developed to provide a practical tool for engineering design. To ensure a robust evaluation and avoid circular logic, the modeling process was divided into two distinct phases. Experiments 1 and 4, representing the extremes of the flow range, were used for parameter identification and model reconstruction, while Experiments 2 and 3 served as independent validation cases.

Table II summarizes the mass flow rates and temperature conditions for each case. The Richardson number (Ri) was calculated using Eq. (17), with an inlet diameter of 0.0075 m and gravity g = 9.81 m/s². Experiments 1 and 2 were conducted under low Ri conditions (Ri = 0.01 and 0.04 indicating that inertial mixing dominated over buoyancy-driven stratification [25, 26]. In contrast, Experiments 3 and 4 reached Ri values approaching the half critical Ri = 3.6 according to Rendall [16] for thermal stratification (Ri = 0.7 and 1.7), where buoyancy effects became more pronounced, although active mixing was still observed [27–29].

TABLE II. Experimental Conditions and Calculated Parameters for Richardson Number

Exp.	$\dot{m}_h$ (kg/s)	T_0 (°C)	T_f (°C)	T_c (°C)	Ri
1	95×10^{-3}	33.4	14.1	7.9	0.01
2	48×10^{-3}	33.0	16.6	7.3	0.04
3	11×10^{-3}	33.1	23.9	7.8	0.7
4	7.2×10^{-3}	34.4	26.0	8.7	1.7

Since the primary loop lacks a flow meter, the mass flow ratio was derived from Eq. (1) as follows:

$$T_{c,o}(t) - T_c(t) = \frac{\dot{m}_h}{\dot{m}_c}[T(t) - T_{h,o}(t)] \tag{22}$$

The mass flow ratio for Experiment 1 is determined by the slope of the temperature difference on the cooling side versus the heating side. For this condition, the calculated values are $\dot{m}_h/\dot{m}_c$ = 0.593 and $\dot{m}_c$ = 0.160 kg/s. It should be noted that at small temperature differences, the calculated ratio may be subject to uncertainty due to sensor noise. Therefore, the ratios for the remaining cases were determined directly using $C_r = \dot{m}_h/\dot{m}_c$ based on the constant $\dot{m}_c$ = 0.160 kg/s.

B. Identification of Heat Exchanger Characteristics

This section characterizes the thermal performance of the plate heat exchanger through a dual-stage approach: a phenomenological study to verify steady-state assumptions and the development of a predictive mathematical model for heat transfer coefficients.

First, a phenomenological study was performed to evaluate the validity of the quasi-steady-state assumption across the experimental range. In this study, the plate heat exchanger was configured for counter-flow operation. A steady-state ε–NTU model for a counter-flow concentric heat exchanger is employed to characterize the thermal performance, as defined by the following expression:

$$\varepsilon = \frac{1-\exp(-NTU(1-C_r))}{1-C_r \cdot \exp(-NTU(1-C_r))} \tag{23}$$

Fig. 5 compares the effectiveness and NTU values calculated via Eq. (23) with the instantaneous values derived from experimental data. Experimental effectiveness is calculated using Eq. (6) with $\dot{m}_{min} = \dot{m}_h$ while the NTU is obtained from Eq. (9) using the UA value derived from Eqs. (2) and (3) as follows:

$$UA = \frac{\dot{m}_h C_p (T - T_{h,o})}{\text{LMTD}} \tag{24}$$

The experimental results demonstrate that the instantaneous values align closely with the steady-state ε-NTU model, supporting the quasi-steady-state assumption for the tested operating range. This finding suggests that designers can utilize the simpler steady-state ε-NTU framework to accurately predict heat transfer performance, even under transient operating conditions.

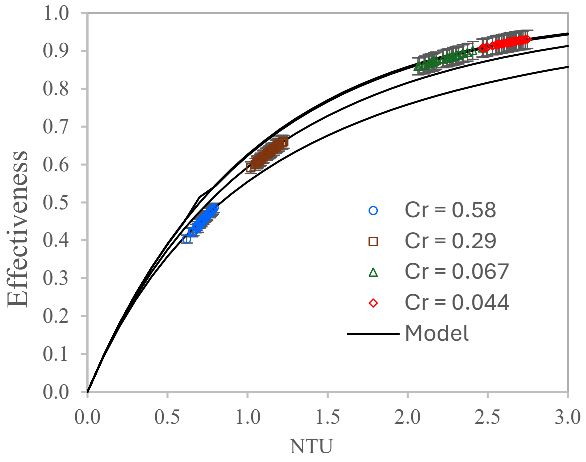

Fig. 5. Comparison of experimental and modeled effectiveness versus NTU for various heat capacity ratios.

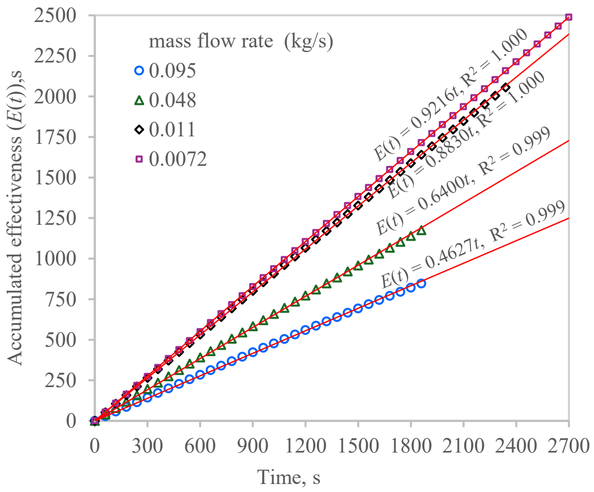

Fig. 6. Time-dependent variation of accumulated effectiveness at different mass flow rates.

The time-dependent variation of accumulated effectiveness is shown in Fig. 6. These values are computed through numerical integration using the trapezoidal rule according to

$$E(0) = 0,\ E(t_k) = E(t_{k-1}) + \frac{\varepsilon(t_k) + \varepsilon(t_{k-1})}{2}(t_k - t_{k-1}) \quad (25)$$

where t_k represents the discrete time at step k. The experimental results illustrated in Fig. 6 demonstrate a strong linear correlation between the accumulated effectiveness and time for all tested mass flow rates. This linear behavior is further confirmed by the coefficient of determination (R^2), the values of which are approximately unity in all cases. Since the accumulated effectiveness represents the integral of instantaneous effectiveness over time, the slope of each line effectively represents the time-averaged effectiveness for that specific operating condition. Based on Eq. (14), the accumulated effectiveness can be expressed as $E(t) = \bar{\varepsilon}t$ The time-averaged effectiveness values, $\bar{\varepsilon}$ were found to be 0.4627, 0.6400, 0.8830, and 0.9126, corresponding to hot-stream mass flow rates $\dot{m}_h$ of 0.095, 0.048, 0.011, and 0.0072 kg/s, respectively.

Following the physical verification, a predictive model is established by identifying empirical constants from Experiments 1 and 4, while Experiments 2 and 3 are reserved for independent validation of the UA and effectiveness predictions.

The overall heat transfer coefficient, U, can be approximated by considering the thermal resistances of both the hot and cold fluid streams. Neglecting the conductive resistance of the plate, the relationship is expressed as:

$$\frac{1}{UA} \approx \frac{1}{h_h A} + \frac{1}{h_c A} \quad (26)$$

where h_h and h_c denote the convective heat transfer coefficients for the hot and cold sides, respectively. For turbulent flow in a tube, the Nusselt number: Nu [29] is typically modeled as:

$$\mathrm{Nu} = 0.023\ \mathrm{Re}^{0.8}\mathrm{Pr}^{1/3} \quad (27)$$

where Re represents the Reynolds number, and is turbulent flow. Moreover, Pr is the Prandtl number and $0.6 < \mathrm{Pr} < 160$. Substituting the definitions of the Reynolds and Nusselt numbers into the equation and assuming nearly constant fluid properties over the operating temperature range, the convective heat transfer coefficient becomes a function of the mass flow rate, such that

$$h_h = B_h \dot{m}_h^{0.8},\ \ h_c = B_c \dot{m}_c^{0.8} \quad (28)$$

In this context, B_h and B_c serve as a grouping constant that incorporates the fluid's thermal properties and the exchanger's geometric characteristics.

By substituting Eq. (28) into Eq. (26), the overall thermal resistance $(UA)^{-1}$ can be expressed as

$$\frac{1}{UA} \approx \frac{1}{B_h A}\dot{m}_h^{-0.8} + \frac{1}{B_c A}\dot{m}_c^{-0.8} \quad (29)$$

In the current experimental setup, the cold stream mass flow rate $\dot{m}_c$ was maintained at a constant value across all test cases. Consequently, the relationship shows that $1/(UA)$ varies linearly with $\dot{m}_h^{-0.8}$. The grouped constant terms, $(B_h A)^{-1}$ and $(B_c A)^{-1}\dot{m}_c^{-0.8}$, can therefore be determined through linear regression of the experimental data.

The heat exchanger characteristics are summarized in Table III, where the time-averaged overall thermal conductance, $\overline{UA}$ was experimentally determined using Eq. (24). By utilizing the data from Experiments 1 and 4 to identify the empirical constants in Eq. (29), the following predictive model was established:

$$(UA)^{-1} = 0.1936\dot{m}_h^{-0.8} + 2.0833 \quad (30)$$

Furthermore, Experiments 2 and 3 were utilized to validate the model. The UA values obtained from Eq. (30) are in good agreement with the experimental results. The NTU was then calculated using Eq. (9) based on the parameters established in Eq. (28). Additionally, the predicted effectiveness, $\bar{\varepsilon}$, was determined by Eq. (23). These predicted values of $\bar{\varepsilon}$ were in close agreement with the time-averaged effectiveness derived from Fig. 6, further validating the consistency of the experimental data.

TABLE III. HEAT EXCHANGER CHARACTERISTICS

Exp.	$\dot{m}_h$(kg/s)	$\overline{UA}$	UA	C_r	NTU	$\bar{\varepsilon}$
1	0.095	0.298	0.298	0.58	0.75	0.468
2	0.048	0.235	0.234	0.29	1.16	0.644
3	0.011	0.114	0.109	0.067	2.35	0.895
4	0.0072	0.083	0.083	0.044	2.74	0.930

C. *Validation of the Transient Model for a Mixing Assumption Tank*

This section evaluates the tank cooling dynamics by investigating the influence of the Richardson number (Ri) on mixing behavior and thermal stratification. Using the experimental dataset, the phenomenological limits of the mixed-state assumption were identified. Fig. 7 illustrates the temperature profiles from all ten sensors over the 30-minute test duration and includes the measured cold-side inlet temperature (T_c) profiles. During the tests, T_c remained within approximately 7–9 °C, with only minor fluctuations. These variations were negligible compared with the overall decrease in tank temperature from about 30–35°C to the final temperature.

Fig. 7(a) and 7(b) show nearly identical readings for sensors 2 through 10 (the average maximum temperature differences over time are 0.42 and 0.45 °C, respectively), while sensor 1 is slightly lower due to its proximity to the incoming cold stream. This confirms a well-mixed condition at low Ri values (0.01 and 0.04). As Ri increases to 0.7 and 1.7 in Fig. 7(c) and 7(d), a slight spatial divergence emerges between the upper (sensor 1) and lower (sensor 10) sections, where the average maximum temperature differences over time are 1.6 and 1.2 °C. Although these absolute spatial temperature differences show no significant or drastic separation between the low and high Ri cases, the influence of the Richardson number becomes distinctly apparent when evaluating the maximum temperature difference relative to the overall average temperature drop (which yields 2.4%, 2.9%, 24.8%, and 28.5%, respectively). This relative metric uncovers a direct physical coupling; with a constant inlet cross-sectional area, the overall cooling capacity varies systematically with the kinetic energy of the injection (u^2), which simultaneously governs the denominator of both the Ri definition and the normalized temperature drop. Ultimately, this bounded nature of profile separation demonstrates that inertial mixing still dominates buoyancy forces, maintaining a mixing state without distinct thermal stratification at these specific Ri values. This is consistent with previous studies demonstrating that mixing processes continue to dominate even at Ri < 3.6 [16]. Therefore, the four tested cases remained within conditions where no distinct thermal stratification was observed, making the mixed-tank assumption defensible for the present experimental range.

Following the physical verification of the mixing regimes, the quantitative validation of the transient thermal model has been focused on. By substituting the effectiveness values from Table III into Eq. (15), using the relationship $E(t) = \bar{\varepsilon}t$, the time-dependent temperature decrease of the mixed tank can be predicted. To account for the thermal inertia of the system, an equivalent water mass, M, was determined from the measured water mass and tank mass according to the relation $M = (M_{water}C_p + M_{tank}C_{tank})/C_p$. With M_{water}= 53.1 kg, M_{tank} = 17 kg, and the specific heat capacities for water (C_p = 4.186 kJ/kg·K) and the stainless-steel tank (C_{tank} = 0.5 kJ/kg·K), the resulting equivalent mass is calculated as M = 55.13 kg. The accuracy of the proposed transient model in estimating the thermal behavior of the tank cooling is demonstrated through a comparison with experimental data across varying flow conditions.

As illustrated in Fig. 7(a) and 7(b), the temperature profiles predicted by Eq. (15) demonstrate a high degree of accuracy. In Fig. 7(a), the model successfully reconstructs the experimental data used during the parameter identification phase, yielding an R^2 value of 0.9978, excluding sensor 1. More importantly, Fig. 7(b) presents an independent prediction for a flow rate not used in the initial identification. The model shows the exponential decay for this case with R^2 of 0.9944, excluding sensor 1, showing exceptional agreement with the uniform sensor readings. This consistency between the reconstructed experiment in Fig. 7(a) and the independent validation experiment in Fig. 7(b) at low Ri values (0.01 and 0.04) indicates that the model is well calibrated and can reliably predict the cooling trend within the tested low-Ri range.

Even at higher Richardson numbers, where minor spatial temperature deviations emerge, the model remains effective at predicting the bulk-water temperature evolution. As shown in Fig. 7(d), which represents the upper extreme of the flow range (Ri = 1.7) used for parameter identification, the model reconstructs the cooling profile with an R^2 of 0.8738. Crucially, in Fig. 7(c), the model provides an independent prediction for an intermediate flow condition (Ri = 0.7). Despite the increased complexity of the mixing behavior, the predicted profile in Fig. 7(c) aligns closely with the experimental data, yielding a higher R^2 value of 0.9392, including sensor 1.

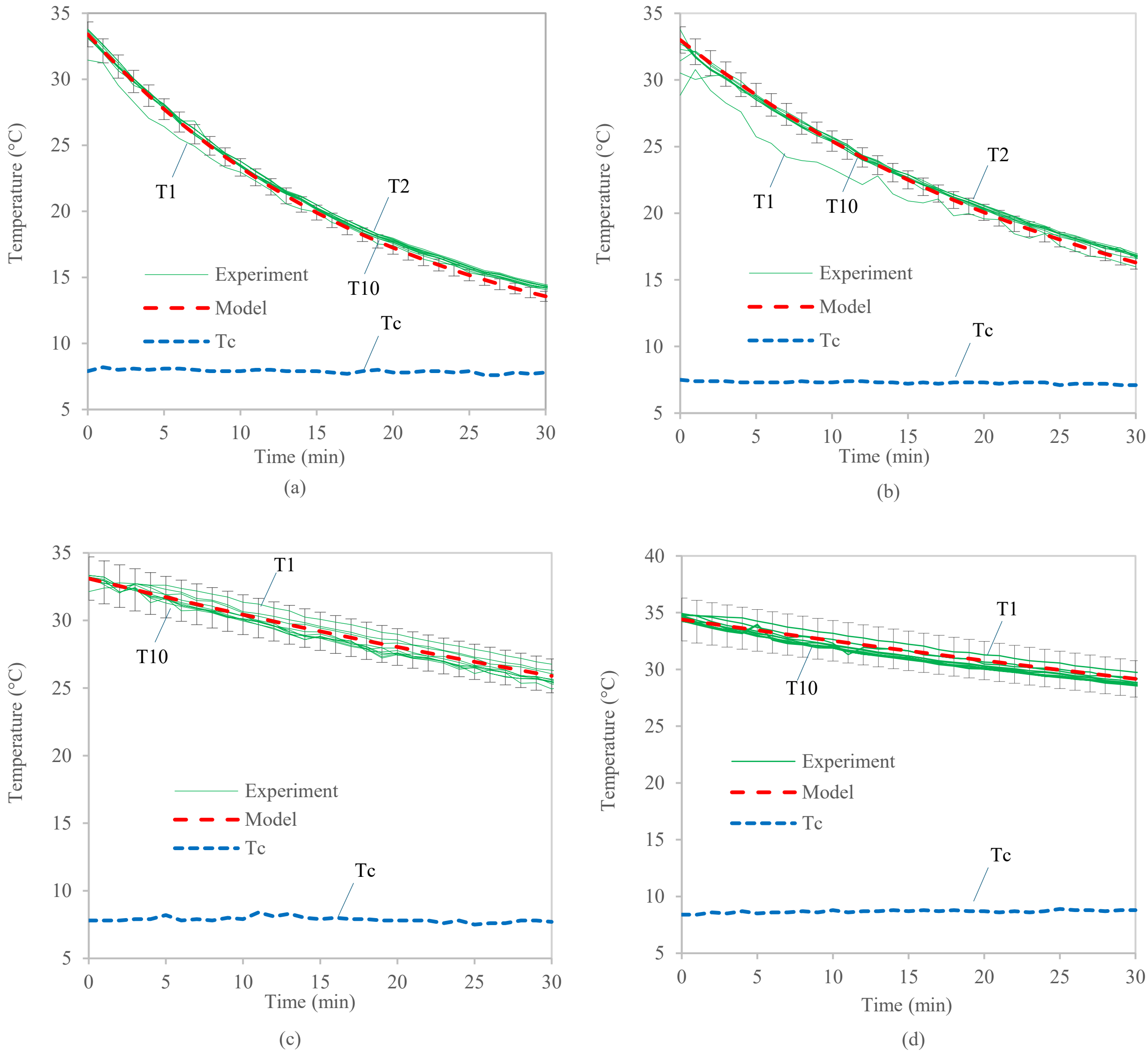

Fig. 7. Comparison between predicted and measured tank temperatures using time-dependent and constant effectiveness models. (a) Flow rate 0.095 kg/s; (b) Flow rate 0.048 kg/s; (c) Flow rate 0.011 kg/s; (d) Flow rate 0.0072 kg/s.

The agreement between the theoretical predictions and experimental measurements indicates that the ε-NTU-based transient model can reasonably predict bulk-water temperature over the tested operating range. These results support the use of the quasi-steady-state heat exchanger assumption combined with the mixed tank model. This approach is particularly applicable under low-Ri conditions and transitional cases where no distinct thermal stratification is observed.

IV. Discussion

A key finding of this study is the validity of the quasi-steady-state assumption applied to the heat exchanger effectiveness. In theory, the effectiveness $\varepsilon(t)$ depends on temperature-dependent fluid properties and therefore varies with time. However, the experimental results indicate that treating effectiveness as constant is reasonable over the tested operating range. The primary reason is the relatively narrow operating temperature range, as the water was cooled only from 35 °C to 15 °C. Although variations in the thermophysical properties of water do affect the overall heat transfer coefficient within this 20 °C span, their cumulative effect on the time-averaged effectiveness was small for the tested conditions.

These observations indicate that assuming a constant effectiveness is appropriate for design purposes in systems operating under low Richardson number conditions, such as rapid chilled-water production. The simplification also reduces the computational complexities, while still providing reliable estimates of the cooling rate and, in turn, the required chiller and heat exchanger capacities.

To avoid concerns regarding a circular workflow, the model evaluation was separated into identification and validation phases. Fig. 7(a) and 7(d) use the extremes of the experimental flow range to establish the model's coefficients, while Fig. 7(b) and 7(c) provide independent validation through interpolated flow rates. Good agreement was observed across this range that supports the predictive capability of the model. However, the limitation is the large intervals between the selected Richardson numbers (Ri = 0.01, 0.04, 0.7, and 1.7), which makes it difficult to identify the exact transition threshold where the mixing assumption may begin to deviate. Despite this lack of resolution, the study covers typical operating conditions, and the model is sufficiently accurate for practical engineering design and performance estimation.

The generalizability of the proposed model is supported by both its theoretical foundation and the range of experimental conditions examined. The governing equations are derived from fundamental heat transfer principles, the ε-NTU method, and the energy balance. They are independent of both geometry and specific configuration. This allows the model to predict the trends of thermal response with reasonable reliability across different system configurations. The present study was conducted with a limited number of experiments. However, the applicability of the ε-NTU formulation is expected to apply to other heat exchanger types. This applicability holds provided the appropriate effectiveness relation and heat capacity rate ratio for the configuration of interest are used.

The predictive relations remain useful when the Richardson number is low enough to maintain a mixed tank. However, tank geometry, inlet configuration, and aspect ratio should be considered when applying the model to systems outside the tested range. In systems where the refrigerant temperature can be held reasonably constant, the model can also be extended to direct-cooling arrangements, in which the evaporator cools the tank water directly. The high R^2 values observed across all test cases, these factors support the use of the proposed model as a practical tool for chilled-water system designs.

The following procedure provides a streamlined framework for sizing chilled-water systems based on the validated transient model. When the cold-water storage tank is designed with a low Richardson number, the temperature difference between the top and bottom of the tank is minimal. Consequently, Eq. (16) can be used to estimate the final tank temperature, even when the effectiveness is assumed to be constant. Therefore, the temperature prediction model derived from Eq. (16) can be applied to determine the required chiller capacity and serve as a basis for designing the heat exchanger. If the objective is to produce chilled water with a total mass M, reducing its temperature from an initial temperature T_0 to a target temperature T_f within a specified time duration t_f, the system can be designed according to the following procedure.

(1) The type of heat exchanger and the desired effectiveness ε should be selected. Then, the outlet chilled water temperature from the chiller, T_c, must be specified. The chilled water flow rate can be approximated from Eq. (16) as

$$\dot{m}_{min} \approx \frac{M}{\varepsilon t_f} \ln\left(\frac{T_0-T_c}{T_f-T_c}\right) \tag{31}$$

(2) After specifying the tank height, calculate the Richardson number (Ri) using Eq. (17) to verify whether the Ri value falls within the acceptable range, thereby confirming that thermal mixing occurs within the tank.

(3) The required heat exchange rate can then be calculated using:

$$Q = \varepsilon \dot{m}_{\min} C_p (T_0 - T_c) \tag{32}$$

By substituting Eq. (31) into the equation, the heat transfer rate can be rewritten as:

$$Q = \frac{MC_p}{t_f}(T_0 - T_f)\left(\frac{T_0-T_c}{T_0-T_f}\right)\ln\left(\frac{T_0-T_c}{T_f-T_c}\right) \tag{33}$$

For comparison, the conventional approach estimates heat exchange rate using the following equation:

$$Q = \frac{MC_p}{t_f}(T_0 - T_f) \tag{34}$$

From Eqs. (33) and (34), a correction factor ϕ can be defined as

$$\phi = \left(\frac{T_0-T_c}{T_0-T_f}\right)\ln\left(\frac{T_0-T_c}{T_f-T_c}\right) \tag{35}$$

The correction factor ϕ is defined as the ratio between the heat transfer rate obtained from the transient formulation and that estimated from the conventional steady-state energy balance. Under the condition $T_0 > T_f > T_c$, the logarithmic term in Eq. (35) yields ϕ greater than unity. This indicates that the heat transfer rate estimated from the transient formulation is higher than that obtained from the steady-state estimate for the same cooling duration. The value of ϕ depends on the selected operating temperatures. For example, when T_0 = 30 °C, T_f = 15 °C, and T_c = 7 °C, Eq. (35) gives ϕ = 1.6. As T_c approaches T_f, the available temperature difference decreases and ϕ increases accordingly.

(4) The calculated flow rate and heat exchange rate can be used to design the heat exchanger using either the Logarithmic Mean Temperature Difference (LMTD) method or the NTU method, depending on design preferences. Moreover, any type of heat exchanger can be selected, as the conditions used in the equations apply to all types. Assuming negligible heat loss from equipment or piping, the minimum required chiller capacity is equal to the calculated heat exchange rate.

(5) Eq. (31) can also be applied to systems in which the water in the tank is directly cooled by a chiller, provided that the refrigerant temperature remains constant. In this case, the heat exchanger is considered to be the evaporator of the chiller, and the refrigerant temperature is represented by T_c.

Example calculation: To demonstrate the application of Eqs. (31)–(35), consider a 5 m^3 water tank (approximately 5000 kg of water) that must be cooled from 30 °C to 15 °C within 30 minutes using chilled water at 7 °C. For practical design calculations, the constant effectiveness value is determined from the average thermal conditions: $T_{avg} = (T_0 + T_f)/2 = (30+15)/2 = 22.5$ °C. Assuming a heat exchanger effectiveness of ε = 0.7 at this average temperature and a specific heat capacity of water taken as 4.18 kJ/(kg·K) and substituting these values into Eq. (31) yields a minimum mass flow rate of 4.19 kg/s. From Eq. (32), the corresponding heat transfer rate is Q = 282 kW, representing the minimum required chiller capacity. The correction factor from Eq. (35) is $\phi = 1.6$ for this specified operating condition. For comparison, the conventional steady-state approach in Eq. (34) gives a heat transfer rate of 174 kW. This constant-effectiveness approach is validated by results and significantly simplifies the design procedure. For heat exchanger sizing, assuming a conventional chiller with a temperature difference of 5.56 °C yields a maximum chiller-side mass flow rate of 12.14 kg/s. This corresponds to a heat capacity ratio Cr = 0.34. This Cr value can then be used to determine the required NTU from standard heat exchanger correlations for the selected exchanger type, such as plate or shell-and-tube, which directly yields the required heat transfer area. This example demonstrates the model's applicability for rapid chilled-water generation systems and highlights its capability to ensure accurate equipment sizing, thereby supporting process reliability while avoiding the costly consequences of undersized chillers.

V. Conclusion

This study presents a predictive mathematical model and a practical tool to determine the appropriate chiller capacity in tank-based chilled-water generation systems requiring rapid cooling under mixing conditions. The model is based on two key physical assumptions. The first is the quasi-steady-state behavior of heat exchanger effectiveness, and the second is the thermal stratification relative to the Richardson number (Ri) remaining below the critical threshold. To validate the proposed model, a two-loop experimental system was constructed. The system comprised a plate heat exchanger coupled with a 3-kW mini chiller and a single 60-L tank designed to rapidly generate chilled water within. Experiments were conducted across a range of flow rates (0.0072–0.095 kg/s) and low Richardson numbers (Ri = 0.01–1.7), under which no distinct thermal stratification was observed. The experimental data were used to verify the accuracy of the model and to examine the time-dependent behavior of heat exchanger effectiveness as well as the Number of Transfer Units (NTU). The key findings and contributions of this study are as follows:

(1) The heat exchanger effectiveness can be treated as quasi-steady throughout the cooling process, as the relatively narrow operating temperature range produces negligible variation in the thermophysical properties of water, thereby justifying the constant-effectiveness assumption adopted in the proposed model.

(2) The quasi-steady-state assumption, combined with the mixed tank model, yields a practical and accurate mathematical model for determining the appropriate chiller capacity in rapid chilled-water generation systems. The present results demonstrate that this fundamental framework is reliable and sufficient for engineering design estimation within the tested operating conditions.

(3) By bridging the gap between idealized steady-state calculations and actual transient system behavior, this work enables more accurate equipment sizing, reduces the risk of chiller under-sizing, and ensures that industrial processes requiring rapid chilled-water generation—such as concrete production, aquaculture, and metal processing—can reliably meet their time-critical operational requirements.

Nomenclature

A	heat exchange area of heat exchanger	[m^2]
C_p	specific heat of water	[kJ/(kg·K)]
C_{max}	maximum heat capacity rate	[kW/°C]
C_{min}	minimum heat capacity rate	[kW/°C]
C_r	heat capacity ratio (C_{min}/C_{max})	
g	gravitational acceleration	[m/s^2]
H	tank height	[m]
LMTD	log-mean temperature difference	[°C]
$\dot{m}$	mass flow rate	[kg/s]
$\dot{m}_{min}$	minimum mass flow rate	[kg/s]
NTU	number of Transfer Units	
Q	heat transfer rate	[kW]
Ri	Richardson number	
T	water temperature	[°C]
T_0	initial water temperatures in tank	[°C]
T1-T10	water temperatures measured by thermocouples 1–10 in the tank [°C]	
T_f	final water temperatures in tank	[°C]
T_c	chilled water supply temperature	[°C]
t	time	[s]
u_{in}	inlet water velocity to tank	[m/s]
UA	overall conductance	[kW/°C]
$E(t)$	the time-dependent accumulated effectiveness	

Greek Letters

β	coefficient of thermal expansion	[1/°C]
ε	effectiveness of heat exchanger	
$\bar{\varepsilon}$	the time-averaged effectiveness	
ε_0	nominal effectiveness of heat exchanger	
$\varepsilon(t)$	time-dependent effectiveness	
ϕ	correction factor	

Subscripts

0	initial
C	cold water loop
exp	experimental
f	final
h	warm water loop
i	inlet
max	maximum
min	minimum
o	outlet

Conflict of Interest

The authors declare that they have no known competing financial interests or personal relationships that could have appeared to influence the work reported in this paper.

Author Contributions

N.K.: Writing—review & editing, Writing—original draft, Conceptualization, Visualization, Validation, Methodology, Investigation, Formal analysis, Data curation.; W.F.: Writing—review & editing, Writing—original draft, Conceptualization, Methodology, Investigation, and Formal analysis. S.A.: Methodology, investigation.; R.A.: Writing—review & editing, Writing – original draft, Validation, Methodology, Formal analysis, Conceptualization, Data curation and project administration. All authors have read and agreed to the published version of the manuscript.

Funding

This study was supported by the University of Phayao and the Thailand Science Research and Innovation Fund (Fundamental Fund 2026 Grant No. 2374).

References

[1] Cement Australia Pty Ltd. (Mar. 18, 2011). *Low Heat Cement Product Data Sheet*. Darra, QLD, Australia: Cement Australia. [Online]. Available: https://www.cementaustralia.com.au

[2] M. Assal and M. N. Abou-Zeid, "The effect of mixing water temperature on concrete properties in warm weather conditions," in *Proc. CSCE Annu. Conf.—MA20: Building Tomorrow's Society*, Fredericton, Canada, 2018, Jun. 13–16.

[3] GCP Applied Technologies Inc. (2016). *Warm Weather Concrete: Technical Bulletin TB-0101*, Cambridge, MA, USA. [Online]. Available: https://gcpat.com

[4] T. J. Snow Company. How to correctly size a chiller. [Online]. Available: https://tjsnow.com/resistance-welding-supplies/water-chiller/how-to-correctly-size-a-chiller/

[5] Conair Group. Chiller sizing, Part 2—The Old School Way. *Resources: Technical Article*. [Online]. Available: https://www.conairgroup.com/resources/resource/chiller-sizing-part-2-the-old-school-way/

[6] J. D. Chung, S. H. Cho, C. S. Tae, and H. Yoo, "The effect of diffuser configuration on thermal stratification in a rectangular storage tank," *Renew. Energy*, vol. 33, no. 10, pp. 2236–2245, 2008.

[7] D. R. Parida, S. Advaith, N. Dani, and S. Basu, "Assessing the impact of a novel hemispherical diffuser on a single-tank sensible thermal energy storage system," *Renew. Energy*, vol. 183, pp. 202–218, Jan. 2022.

[8] M. W. K. Jaber, A. Güngör, E. Canli, A. H. Abdulkarim, and U. Sentürk, "Transient evolution of thermal stratification and passive flow guidance inside a heat exchanger immersed thermal energy storage tank," *J. Energy Storage*, vol. 88, 111472, May 30, 2024.

[9] U. Stritih, "An experimental study of enhanced heat transfer in rectangular PCM thermal storage with water as a heat transfer fluid," *Int. J. Heat Mass Transfer*, vol. 47, no. 12–13, pp. 2841–2847, 2004.

[10] A. Sharma, V. V. Tyagi, C. R. Chen, and D. Buddhi, "Review on thermal energy storage with phase change materials and applications," *Renew. Sustain. Energy Rev*., vol. 13, no. 2, pp. 318–345, 2009.

[11] N. Nallusamy, S. Sampath, and R. Velraj, "Experimental investigation on a combined sensible and latent heat storage system integrated with constant/varying (solar) heat sources," *Renew. Energy*, vol. 32, no. 7, pp. 1206–1227, 2007.

[12] Q. Mao, Y. Li, and M. Chen, "Design and investigation of single tank phase change thermal storage domestic hot water system," Case Stud. *Therm. Eng*., vol. 25, 100903, 2021. doi: 10.1016/j.csite.2021.100903

[13] A. Riebel, I. Wolde, R. Escobar, R. Barraza, and J. M. Cardemil, "Transient modeling of stratified thermal storage tanks: Comparison of 1D models and the advanced flowrate distribution method," *Case Stud. Therm. Eng.*, vol. 61, 105084, 2024. doi: 10.1016/j.csite.2024.105084

[14] A. Karim, A. Burnett, and S. Fawzia, "Investigation of stratified thermal storage tank performance for heating and cooling applications," *Energies*, vol. 11, no. 5, 1049, 2018. doi: 10.3390/en11051049.

[15] A. J. Osiadacz, Ł. Kotyński, and M. Kwestarz, "A comparative study of one-dimensional models for stratified thermal energy storage," *Gaz, Woda i Technika Sanitarna*, no. 9, pp. 8–14, 2023, doi: 10.15199/17.2023.9.2

[16] J. Rendall, A. Abu-Heiba, K. Gluesenkamp, K. Nawaz, W. Worek, and A. Elatar, "Nondimensional convection numbers modeling thermally stratified storage tanks: Richardson's number and hot-water tanks," *Renew. Sustain. Energy Rev*., vol. 145, 111471, 2021. doi: 10.1016/j.rser.2021.111471

[17] I. Alesbe, H. A. Abdul Wahhab, and S. Aljabair, "Transient study of thermal stratification of full-scale chilled water storage tank during optimum discharge condition," *J. Energy Storage*, vol. 65, 107236, 2023. doi: 10.1016/j.est.2023.107236

[18] Z. Wang, H. Zhang, B. Dou, H. Huang, W. Wu, and Z. Wang, "Experimental and numerical research of thermal stratification with a novel inlet in a dynamic hot water storage tank," *Renew. Energy,* vol. 111, pp. 353–371, 2017. doi: 10.1016/j.renene.2017.04.007

[19] M. S. Saleem and N. Abas, "Optimal design of renewable-driven polygeneration system: A novel approach integrating TRNSYS–GenOpt linkage," *Cleaner Engineering and Technology*, vol. 24, 100856, 2025.

[20] M. S. Saleem and N. Abas, "A solar-assisted grid-tied polygeneration system for hydrogen and electricity production: future of energy transition from electrons to molecules," *Int. J. Hydrogen Energy*, vol. 69, pp. 559–569, 2024. doi: 10.1016/j.ijhydene.2024.05.082

[21] A. Rahman, N. Abas, S. Dilshad, and M. S. Saleem, "A case study of thermal analysis of a solar-assisted absorption air-conditioning system using R-410A for domestic applications," *Case Studies in Thermal Engineering*, vol. 26, 101008, 2021.

[22] F. P. Incropera, D. P. DeWitt, T. L. Bergman, and A. S. Lavine, "Effectiveness–NTU method for heat exchangers," in *Fundamentals of Heat and Mass Transfer*, 6th ed., Hoboken, NJ, USA: Wiley, 2007, pp. 722–730.

[23] T. Gao, B. Sammakia, and J. Geer, "Transient effectiveness methods for the dynamic characterization of heat exchangers," in *Heat Exchangers—Design, Experiment and Simulation, InTech*, 2017, ch. 9, pp. 193–220. doi: 10.5772/67334

[24] R. J. Moffat, "Describing the uncertainties in experimental results," *Int. J. Exp. Heat Transf. Thermodyn. Fluid Mech.*, vol. 1, no. 1, pp. 3–17, 1988.

[25] M. A. Karim, "Experimental investigation of a stratified chilled-water thermal storage system," *Appl. Therm. Eng*., vol. 31, pp. 1853–1860, 2011.

[26] J. S. Turner, *Buoyancy Effects in Fluids*, Cambridge, U.K.: Cambridge University Press, 1973.

[27] J. van Berkel, C. C. M. Rindt, and A. A. van Steenhoven, "Thermocline dynamics in a thermally stratified store," *Int. J. Heat Mass Transf.*, vol. 45, no. 2, pp. 343–356, Jan. 2001.

[28] Y. H. Zurigat, K. J. Maloney, and A. J. Ghajar, "A comparison study of one-dimensional models for stratified thermal storage tanks," *J. Sol. Energy Eng., Trans. ASME*, vol. 111, no. 3, pp. 204–210, 1989.

[29] Y. H. Zurigat, P. R. Liche, and A. J. Ghajar, "Turbulent mixing correlations for a thermocline thermal storage tank," *AIChE SympSer*., vol. 84, no. 263, pp. 160–168, 1988.